Nanoscale

Accepted Manuscript

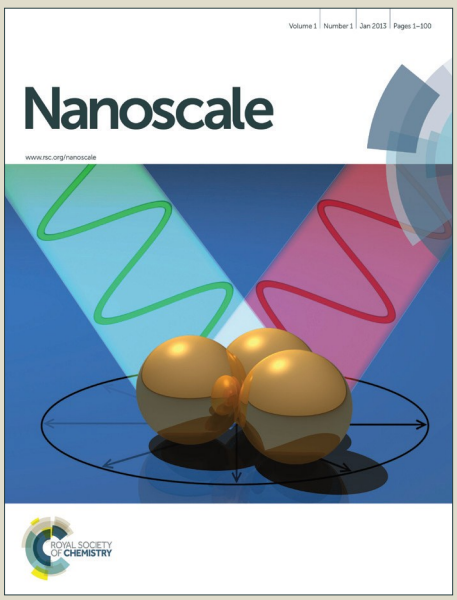

ROYAL SOCIETY OF CHEMISTRY

www.rsc.org/nanoscale

Carbon fiber-ZnS nanocomposite for dual applications as an efficient cold cathode as well as luminescent anode for display technology

Arunava Jha[†,£], Sudipta Kumar Sarkar[†], Dipayan Sen[§], K. K. Chattopadhyay[†,§*]

[†]School of Materials Science and Nanotechnology

[§]Thin Film &Nanoscience Laboratory, Department of Physics,

Jadavpur University, Kolkata 700 032, India

**To whom any correspondence should be addressed*

Abstract:

In the current work we present a simple technique to develop a Carbon nanofiber (CNF) /Zinc sulfide (ZnS) composite material for excellent FED application. CNFs and ZnS microspheres were synthesized by following simple thermal chemical vapor deposition and hydrothermal procedure respectively. A rigorous chemical mixture of CNF and ZnS was executed to produce CNF-ZnS composite material. Cathodo-luminescence intensity of the composite improved immensely compared to pure ZnS. Also, the composite material showed better field emission than pure CNFs. For pure CNF the turn-on was found to be 2.1 V/µm whereas for CNF-ZnS composite it reduced to a value of 1.72 V/µm. Altogether the composite happened to be an ideal element for both anode and cathode of a FED system. Furthermore, simulation analysis for our CNF-ZnS composite system using finite element modeling method also ensured the betterment of field emission from CNF after surface attachment of ZnS nanoclusters.

£ *Author's present address*: St. Thomas College of Engineering and Technology

Introduction

One dimensional carbon nanostructures, e.g. carbon nanotubes (CNTs), carbon nanofibers (CNFs) etc., have always proven to be the most attractive nanomaterial due to their wide applications in the field of nanoelectronics, nanolithography, photovoltaic and field emission displays [1-6]. In recent years functionalization and modification of CNTs and CNFs with organic materials via covalent bonding [7, 8], as well as decoration and composite formation with inorganic material through non-covalent attachment [9, 10] have appeared to be very fruitful for providing new properties which lead to new applications. However non-covalent approaches, which utilize van der Waals interactions between the adjacent materials, has attracted much attention as this can always be expected to enrich the nanocomposite with new properties, but still preserve the respective characteristics of the materials.

In view of this, the optical properties of CNFs can be raised significantly through nanocomposite formation. Zinc sulfide being a wide band-gap (3.6 eV) insulating material is a well-known phosphor element for many cathodoluninescence (CL)-based displays, such as cathode-ray tubes (CRTs), vacuum fluorescent displays (VFD), and field emission displays (FEDs) [11-13]. However it is always better to use a high conducting phosphor in FEDs as it will decrease the charging effect under high voltage and current density. Furthermore, it significantly reduces the decomposition of phosphor as well as thermal quenching caused by a decrease in heat generation on the phosphor surface [14]. The purpose can always be served by developing a nanocomposite system including ZnS and CNFs. Moreover, the presence of CNFs can draw more electrons towards ZnS-based nanocomposite phosphor system, which in-turn can enhance the luminescence capability of the FEDs compared to bare ZnS.

On the other hand presence of ZnS can improve the field emission property of CNF as well. It has been a very common technique in recent days to enhance the field emitting capacity of natural good field emitters like CNTs or CNFs by functionalization and decoration of the outer wall of CNFs with high band-gap nanomaterials. By generating secondary emitter sites on the outer walls, these nanoparticles have always been able to maximize the field emission characteristics of the hybrid system compared to bare CNFs [15-17].

So, in this paper we have developed a new composite material comprised CNFs and ZnS nanoparticle which not only can provide a better luminescent material but also improve the field emission behavior, altogether can serve the dual purpose and make it an ideal element for FEDs.

Experimental Section

Synthesis of CNF: All the reagents used in this experiment were purchased from eMerck and used without further purification. The catalyst supported on copper (Cu) substrate was carried out by simple electro-deposition technique [18]. For this procedure first 2.5 g nickel nitrate [$Ni(NO_3)_2$,$6H_2O$] was taken into 50 ml deionized (DI) water and stirred continuously to make a proper homogeneous solution. 2-3 drops of nitric acid was added to the solution to make it slightly acidic. Cu plates were taken as cathode and an aluminum plate was introduced as anode. Electro-deposition was carried out for 15 min with a fixed current density of 1 mA/cm^2.

Synthesis of CNF on nickel hydroxide deposited substrates was done by thermal chemical vapor deposition procedure. The experimental setup is similar to that described earlier [19]. The Cu plates were placed horizontally inside the quartz tube at high temperature zone. After the reduction of the catalysts in a hydrogen atmosphere at 400^oC for 1 h, acetylene with a flow

rate of 200 sccm was catalytically decomposed at 520^{o}C for 1 h. Finally the deposited black powder on Cu plates was scratched out and collected.

Synthesis of ZnS micro-spheres: ZnS micro-spheres were synthesized by following a simple hydrothermal procedure in which $Zn(O_2CCH_3)_2$ (99.99%) and Thioeurea (99.99%) powders were taken as source for Zn and S respectively. $Zn(O_2CCH_3)_2$ and thioeurea were taken in 1:2 molar ratio by dissolving in DI water and finally mixed well by stirring for some time. The pH value of the solution was kept at 12. The mixed solution was then taken in a Teflon lined autoclave and was tightened strongly enough within a stainless steel made chamber to maintain high pressure. It was then kept in 180^{o} C temperature for 12 hrs to allow the reaction to be completed. Afterwards, the set up was cooled gradually in room temperature and the prepared material was filtered and collected. It was then washed with DI water for several times to wash away the residual impurity and precipitate powders. Finally the as-synthesized material was dried in open air and collected for characterization.

Preparation of CNF-ZnS composite: CNF-ZnS composite material was prepared by a simple mixing procedure which involves a sequence of mixing, evaporation and drying processes. First CNFs and ZnS powder were taken in 1:10 mass ratio and dispersed in dichlorobenzene solvent and sonicated for 1 h. After sonication the suspension was taken in a quartz boat (1 cm x 2 cm), previously washed in acetone, and then heated to 100^{0}C in an air-oven for 15 min to allow solvent evaporation and a fairly accurate cleanness of CNFs. The above procedure was repeated for 3-4 time to improve the homogeneity of the composite.

Characterizations: The as-prepared samples were characterized with X-ray diffraction (XRD, Bruker D8 Advance), field emission scanning electron microscope (FESEM, Hitachi, S-4800)

and high-resolution transmission electron microscope (HRTEM, JEOL-JEM 2100) for structural and morphological analysis. Photo-luminescence (PL) and Cathodo-luminescence (CL) study were done using Elico SL174 and Gatan Mono CL3 equipment attached to FESEM using a beam accelerating voltage of 15 kV respectively. The field emission characteristics of all the samples have been investigated in our laboratory made high vacuum field emission setup.

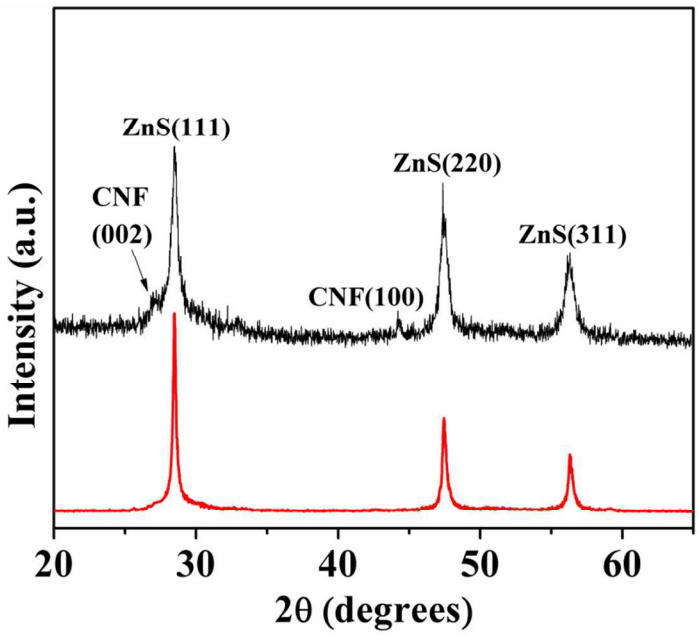

Figure 1. XRD patterns of pure ZnS and CNF-ZnS composite material.

XRD study:

To investigate the crystalline phases of the samples, XRD patterns of pure ZnS and CNF-ZnS composite material are provided in figure 1. For ZnS sample, major peaks appear at 28.46^0, 47.44^0, and 56.30^0 values of 2θ which corresponds to reflections from (111), (220) and (311) planes of cubic ZnS respectively [20]. However for CNF-ZnS composite material two extra peaks have appeared in the XRD pattern at 26.9^0 and 44.25^0 values of 2θ which corresponds to reflections from (002) and (100) planes of hexagonal graphitic phase of carbon confirming the

presence of CNF in the sample. The above XRD analysis ensures proper crystallinity formation of both ZnS and CNF materials.

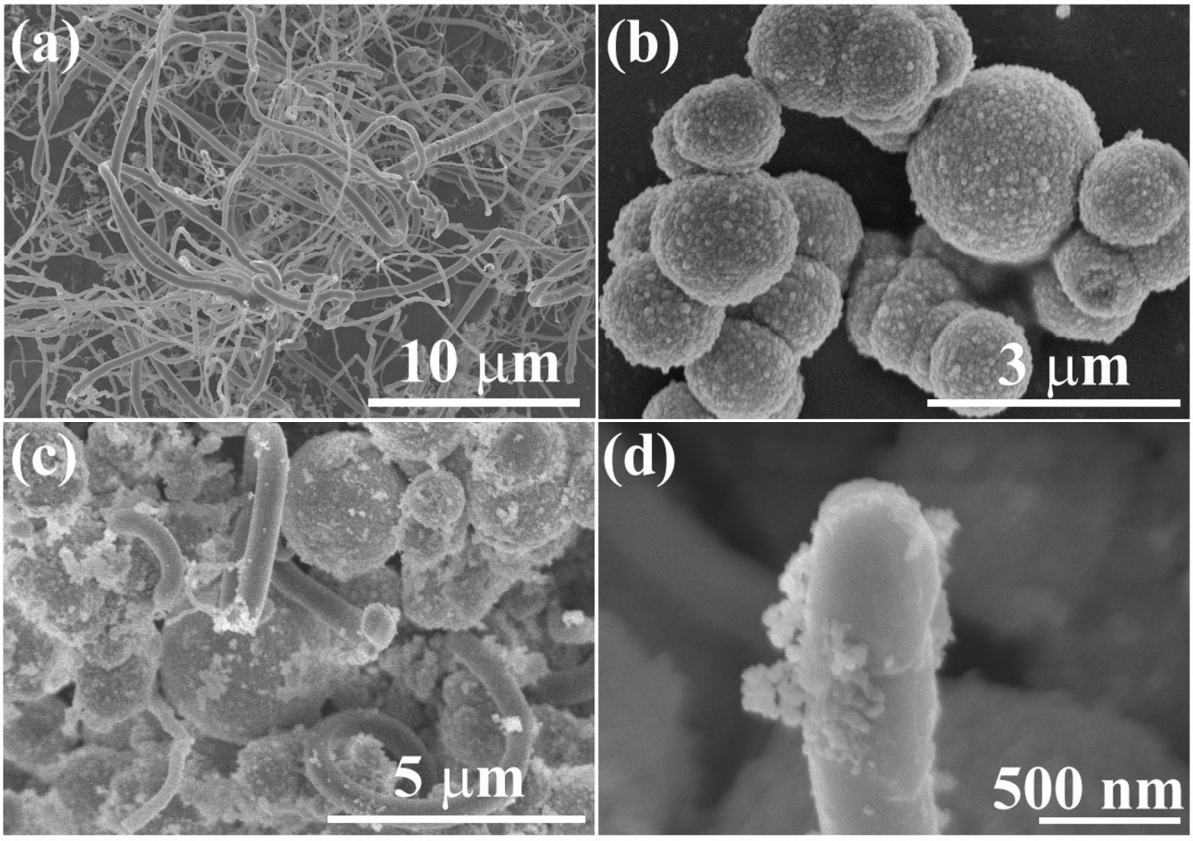

Figure 2. FESEM images of (a) pure CNFs; (b) pure ZnS microspheres; (c) low magnification image of CNF-ZnS composite; (d) high magnification image of CNF-ZnS composite showing ZnS nanoparticles attached to the outer surface of a single CNF.

FESEM analysis :

FESEM images of pure CNF, pure ZnS and CNF-ZnS composite material are illustrated in figure 2. Figure 2a shows the FESEM image of pure CNF powder material where it can be seen that the average diameters of nanofibers are around ~100-150 nm whereas lengths are more than 10 μm. The low magnification image also ensures good yield of the material. FESEM image of pure ZnS

microspheres is provided in figure 2b where it can be observed that the diameters of the microspheres vary in the range ~1-1.5 µm. A minute observation on the spheres clears the fact that a single sphere is actually composed of many ZnS nanoparticles. Finally the FESEM image of the CNF-ZnS composite material is shown in figure 2c where co-presence of both the materials can be viewed clearly.

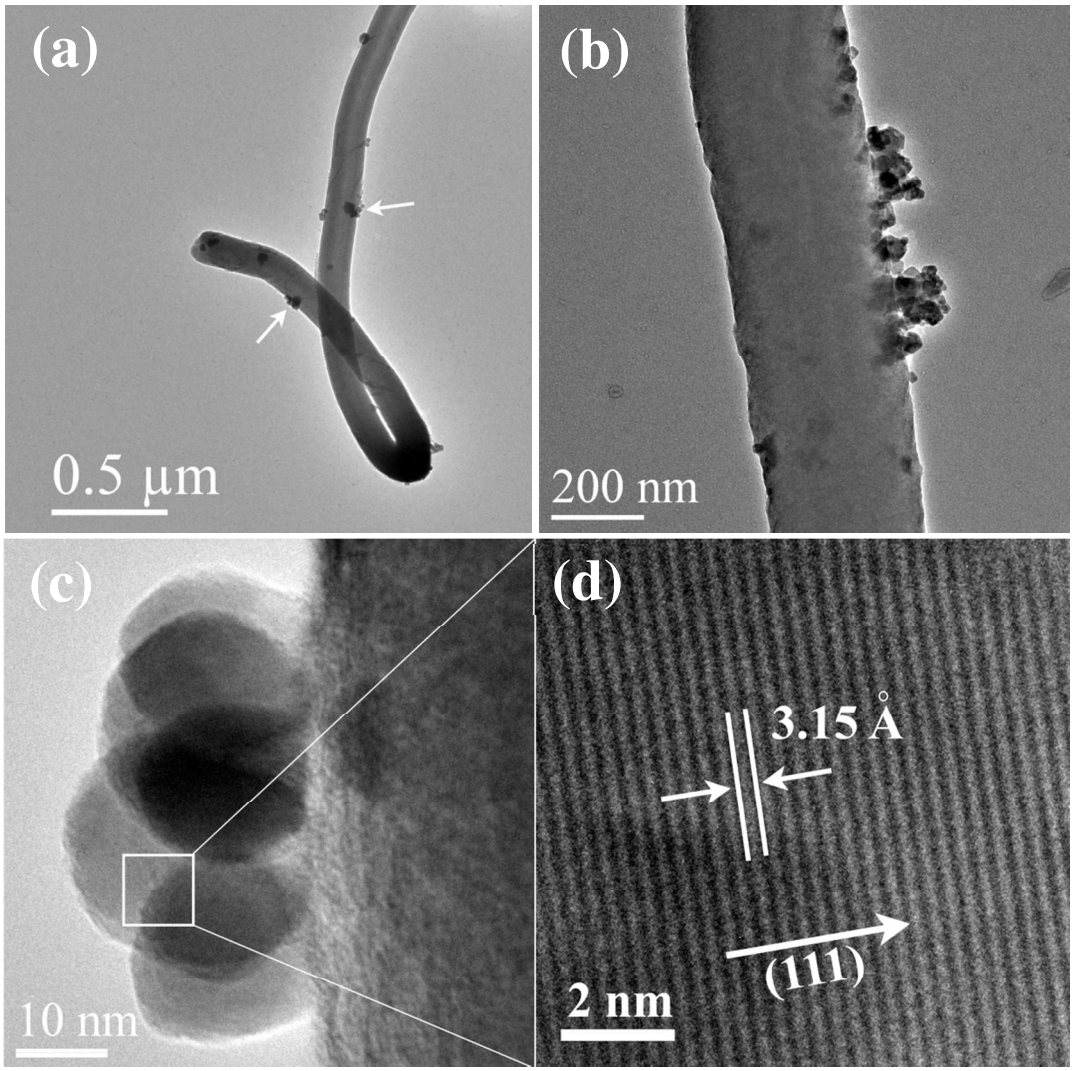

Figure 3. (a) Low magnification HRTEM image of CNF-ZnS composite; (b) A high magnified image of the same showing the attachment of ZnS nanoparticles to the outer surface of CNF; (c) A much higher magnification image indicating the spherical nature of the attached ZnS nanoparticle; (d) lattice image of attached ZnS nanoparticle.

Though the mixture is composed of CNF and ZnS microspheres, during composite preparation some of the ZnS spheres have been broken to their constituent nanopaticles which can be seen attached to the outer surface of the CNFs. A higher magnification image in figure 2d gives a better view of the situation where a large number of ZnS nanoparticles can be seen attached to the outer surface of a CNF. However this kind of attachment is purely physical and governed by vander-waals force of attraction. To further analyze the microstructures of the elements HRTEM study was carried out and provided as follows.

HRTEM analysis :

HRTEM micrographs of CNF-ZnS nanocomposite material are provided in figure 3. Figure 3a shows a single twisted CNF with many small ZnS nanoparticle clusters attached on its surface at different positions as shown by arrow. A higher magnification image given in figure 3b helps in understanding the density and way of attachment of the nanoparticles. A much higher magnified image in figure 3c shows that the average diameters of the attached ZnS nanoparticles are ~20 nm they have been attached in clusters. Figure 3d gives the lattice image of the attached particle. The inter-planar distance, as measured and shown in the image is 3.15 Å which closely matches with that of (111) lattice plane of cubic ZnS appeared in the XRD pattern previously (Figure 1). This observation confirmed the fact that the material is ZnS and attachment is entirely physical.

Luminescence Study:

Photo-luminescence: PL spectra of pure ZnS and CNF-ZnS composite material were recorded with 250 nm excitation wavelength and shown in figure 4a. From the spectra we can have a strong emission band at about 408 nm (3.04 eV) and another weaker peak can be observed at 521

nm (2.38 eV). Usually for semiconductor nano-crystal appearance of two emission peaks is quite natural. The strong and sharp emission peak at 408 nm corresponds to exciton recombination whereas the broad emission peak at 521 nm is called the trapped emission and may be caused by the transition from the conduction band to the zinc vacancies level which is above the valence band at 1.1 eV [21]. It is known that bulk ZnS has the wide direct band gap of 3.68 eV. In present case the shift of emission peak should be attributed to the reduced particle size of ZnS. This shift is the result of a combination of relaxation into shallow trap states and the size distribution [22]. Again it can be seen that incorporation CNF in ZnS results a decrease in the PL intensity for CNF-ZnS material. Evidently black-colored CNF in the ZnS powder functioned negatively as absorbers of excitation and emission lights and therefore lowered the emission intensity.

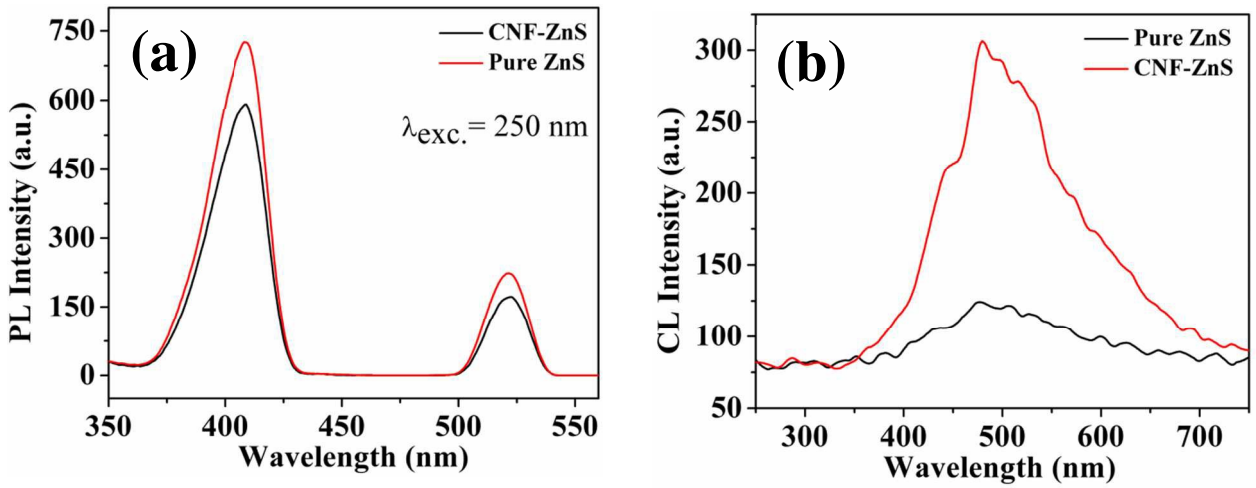

Figure 4. Comparative (a) PL and (b) CL spectra of pure ZnS and CNF-ZnS composite system.

Cathodo-luminescence: CL spectra of pure ZnS and CNF-ZnS composite material is provided in figure 4b. As can be seen from the spectra, both materials exhibit intrinsic green emission at about 478 nm which is caused by ZnS nanoparticles. However, their spectra are red-shifted and

broadened by about 3-4 nm in comparison to PL spectra due to the thermal effect from the heat by the electron bombardment. In contrary to PL spectra, intensity is highly increased for CNF-ZnS composite system compared to pure ZnS due to incorporation of CNF which acted positively in increasing the conductivity of the composite material. Most phosphors, including ZnS, are wide bandgap insulators with low conductivities. In the present scenario, CNF-ZnS composite material delivered better conductivity due to easy electron pathway provided by CNFs. The less accumulation of surface charges near the phosphor surface and the less repulsion of a potential barrier exerted on next incident electrons drastically increased the excited current density and consequently the CL intensity. Additionally, the penetration depth of incident electrons also became higher which in turn increased phosphor layer and volume of excited activators caused enhancement of the CL intensity.

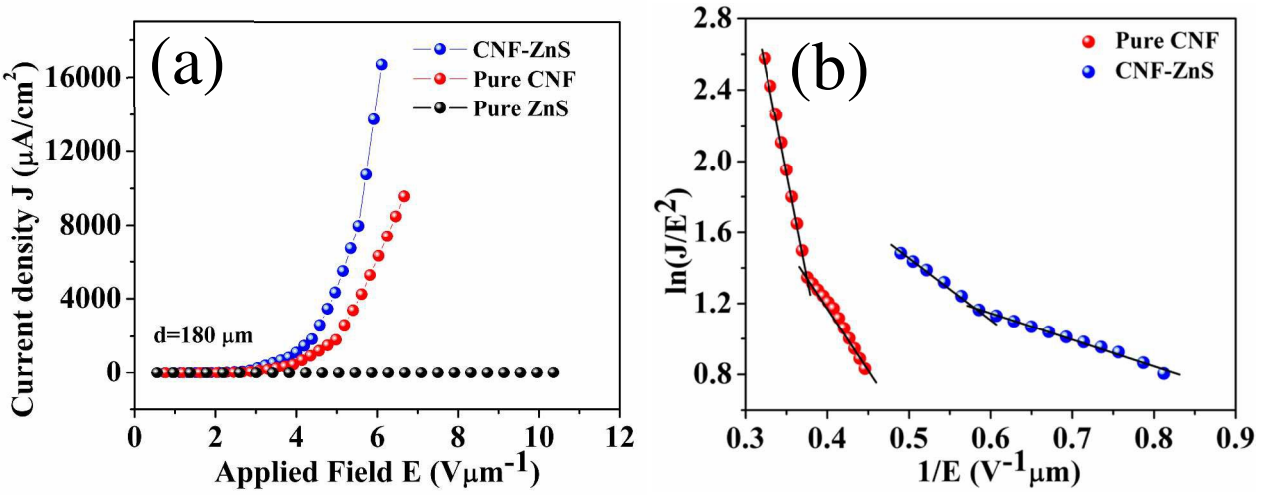

Figure 5. Field emission characteristics; (a) a comparative J-E plot of pure CNF, pure ZnS and CNF-ZnS composite material and (b) corresponding F-N plot.

Field emission study :

To carry out the field emission measurements a laboratory made diode configuration set up consisting of a cathode (powder samples were glued to a conductive carbon tape) and a conical stainless steel anode (1 mm tip diameter) mounted in a liquid nitrogen trapped rotary-diffusion high vacuum chamber with an appropriate chamber baking arrangement. The measurements were performed at a base pressure of ~ 10^{-6} mbar. The tip-sample distance was made adjustable to a few hundred micrometers by means of a micrometer screw. The whole surface of the film was visible through the chamber view port, which enabled us to recognize the electron emission and discharge, if any. It was confirmed that there was no discharge and the current observed due to cold field emission of electron from carbon coils. The size of the sample was ~ 10 mm × 10 mm. Field emitted current density (J) versus applied field (E) curves of pure CNF and CNF-ZnS composite material are shown in Fig 5a. The obtained results were further analyzed using the modified Fowler–Nordheim (F–N) equation [23], which relates the emission current density (J) and applied electric field (E):

$$J = (a\beta^2E^2\varphi^{-1}) \exp(-b\varphi^{3/2} / \beta E) \quad (1)$$

Where a= 1.54 X 10^{-6} A eV V^{-2} and b= 6.83 X 10^7 $eV^{3/2}$ V cm^{-1} are the 1st and the 2nd F-N constants respectively. φ is the work function of the material and β is the enhancement factor relating to the following equation

$$\beta = -b\varphi^{3/2}/S \quad (2)$$

Where S is the slope of the F-N plot, i.e. a plot of $\ln(J/E^2)$ versus 1/E obtained from the modified F-N equation (1). The field emission characteristics are shown in figure 5.

Figure 5a shows comparative J-E plots of pure ZnS microspheres, pure CNF and CNF-ZnS composite material. Inter-electrode distance was kept fixed at 180 µm for both the samples. From the plots it is clear that both pure CNF and CNF-ZnS composite materials exhibit excellent field emission results with very low turn-on field and high emission current density. However it is interesting to note that field emission result of CNFs has got bettered after incorporation of ZnS. From the figure it can also be demonstrated that the threshold field value of 5.67 V/µm is achieved in case of CNF-ZnS where the field emission current density is 1 mA/cm^2, which is generally taken as a standard luminescence parameter for FEDs. However in case of pure CNF the standard threshold field could not be reached. Enhancement in the value of turn-on was also achieved through composite formation with ZnS. The turn-on field was defined as the electric field where the emission current density is 10 µA/cm^2. For pure CNF the turn-on was found to be 2.1 V/µm whereas for CNF-ZnS composite it reduced to a value of 1.72 V/µm. From the comparative graph it is clear that field emission result of pure ZnS microsphere is very poor that its J-E curve appeared almost flat when compared to pure CNF and CNF-ZnS. So, ZnS microspheres contribute insignificantly to the field emission characteristics of the CNF-ZnS composite. Therefore change of concentration of ZnS microspheres present in the composite system, but not attached to CNFs, will not affect significantly to the overall field emission result of the composite material. The F-N plots of pure CNF and CNF-ZnS composite are provided in figure 5b.

F-N plots in figure 5b exhibit two distinct slopes for both pure CNF and CNF-ZnS nano-composite. Both curves have higher slope in the high field region and lower slope in low field region. This phenomena is common in the literature and it is shown by many other semiconducting nanomaterials as reported previously [24,25]. As both CNF and ZnS are well-

known semiconducting nanomaterial, these nonlinearity of FN equations can also be attributed to the semiconducting nature of the emitter. Field emission is a quantum mechanical process based on barrier tunneling and the observed plots are found to obey the FN equation for β factor calculation ($\beta = -b\varphi^{3/2}/S$), where φ is the work function of the emitter material. Taking the work function of CNF and ZnS to be 5 and 7 eV respectively and the β factor has been calculated from the slopes of both low and high field region and given in Table I. The low field region could be attributed to the emission from the conduction band of the materials and high field region corresponds to emission from the valence band (i.e. 3.54 eV below the conduction band in case of ZnS), as well as from the conduction band. The non-linearity can also be attributed to the band bending created due to high field penetration as well as from other defects that may be present in the semiconductor material. In CNF-ZnS nano-composite, electron emission took place mainly due to tunneling of electrons through attached ZnS particles. A significant increase in field enhancement factor (β) is strongly attributed to the geometrical parameters of field emitter, particularly to the radius of curvature of the emitter-tip. The curvature dependency of the field emission enhancement factor (β) has been derived by Edgcombe [26] and he proposed that,

$$\beta \propto \frac{1}{r}$$

where 'r' is the curvature of the emitter tip. It is clear from fesem images that for pure CNFs, emission has been generated from CNF-tip which has much larger radius of curvature compared to the radius of attached ZnS nanoparticles to CNF outer surface in case of CNF-ZnS composite material. Attachment of ZnS roughened the CNF outer surface, which facilitated electric field lines concentration by creating secondary emitter sites and thereby increased the local enhancement factor by a large scale compared to pure CNF. Comparative field emission results

of pure CNF and CNF-ZnS nano-composite have been provided in Table I. It can be seen from Table I that β factor has increased significantly after attachment of ZnS on CNFs. Another aspect of enhanced field emission is the presence of surface states which significantly affected electron field emission. Actually, the emitted electrons have to overcome the surface potential barrier, which depends on the surface states because surface states can trap carriers. Here the presence of ZnS nanoparticles on the outer surface of CNFs served favorable roles for easier electron emission. Since we know that the band-gap of CNF is quite narrow (only a few hundred meV at room temperature) [27], whereas band-gap of ZnS is much wider (3.54 eV). So CNF-ZnS heterojunction can be assumed to similar to that of a metal-semiconductor heterojunction and thus electrons from CNFs can tunnel through the thin Schottky barrier to the conduction band of ZnS under the high external field [28]. The roughness created by ZnS nanoparticles on the smooth outer wall of CNFs enhance the field as clearly shown by simulation results. A lower electron affinity of ZnS (~3.8 eV) compared to CNF (~4.8 eV) [29] provides a very low energy threshold for electrons to escape from the ZnS conduction band to the vacuum. So electrons are more easily emitted from nano-ZnS conduction band to vacuum than from CNFs, which in turn helps in improving field emission characteristics [30,31]. Here, the size of the attached ZnS nano-particles and the local field strength at the top of the particles are the main factors in improving the tunneling effect at the CNF-ZnS junction. It is easier for electrons to tunnel at the boundary of the particles having smaller size, and especially, the higher local field near the nanoparticle emitters can effectively lower the Schottky barrier height at the CNF-ZnS interface, thereby increase the tunneling probability.

The local enhancement factor (β_{loc}) can be derived from the formula $\beta_{loc} = \frac{E_{loc}}{E_{app}}$, where E_{loc} is the local electric field generated and E_{app} is the applied electric field. Taking the local enhancement factor as 15427 and E_{app} as 1.7 V/μm, E_{loc} comes out to be 26 V/nm. As we know field emission is a quantum mechanical process based on barrier tunneling, a high E_{loc} generated on the emitters will help in lowering the barrier width and thereby increase the tunneling probability. Having the average diameters of CNFs to be around ~150 nm with smooth outer surface and average diameters of the attached ZnS nanoparticles to be ~20 nm, there is enough possibility of getting very high field accumulation on the attached nanoparticles which will help in electron tunneling. Previous research suggests that the tunneling of electron is very likely to take place if the barrier width lowered to angstrom (~ Å) order, as there will be certain escape probability of electron tunneling if the De Broglie wavelength of electron matches with that of barrier width. The normal barrier width of ZnS is 8.1 nm [32] which is less probable to allow tunneling. Now application of an external field (F_p) will lower the barrier thickness (x) following the formula, $= \frac{E}{qF_p}$, where q is charge and E is the depth of the surface states of the material [33]. A simpler approximation of generation of a triangular barrier under the application of external field, E can be taken as the work function of the material φ and the above equation becomes, $x = \frac{\varphi}{qF_p}$. Taking φ as 7 eV for ZnS and F_p to be 26 V/nm, the barrier width x comes out as 2.7 Å; which comes out to be realistic. With this reduced value of barrier thickness, electron tunneling is very likely to occur and thereby can produce an improved field emission characteristics.

Field emission simulation and explanation

For 2D simulation of the electric field gradient dispersion for our CNFs and CNF-ZnS composite system we have used Finite element modeling method and ascertained the local electric field dispersion using ANSYS Maxwell software package. The simulations have been carried out according to the following geometrical and material parameterization. For modeling of the CNFs we have chosen graphite with uniform diameter of ~120 nm and length around ~6-7 μm. We have tried our best to configure our system as close as the original system observed from FESEM

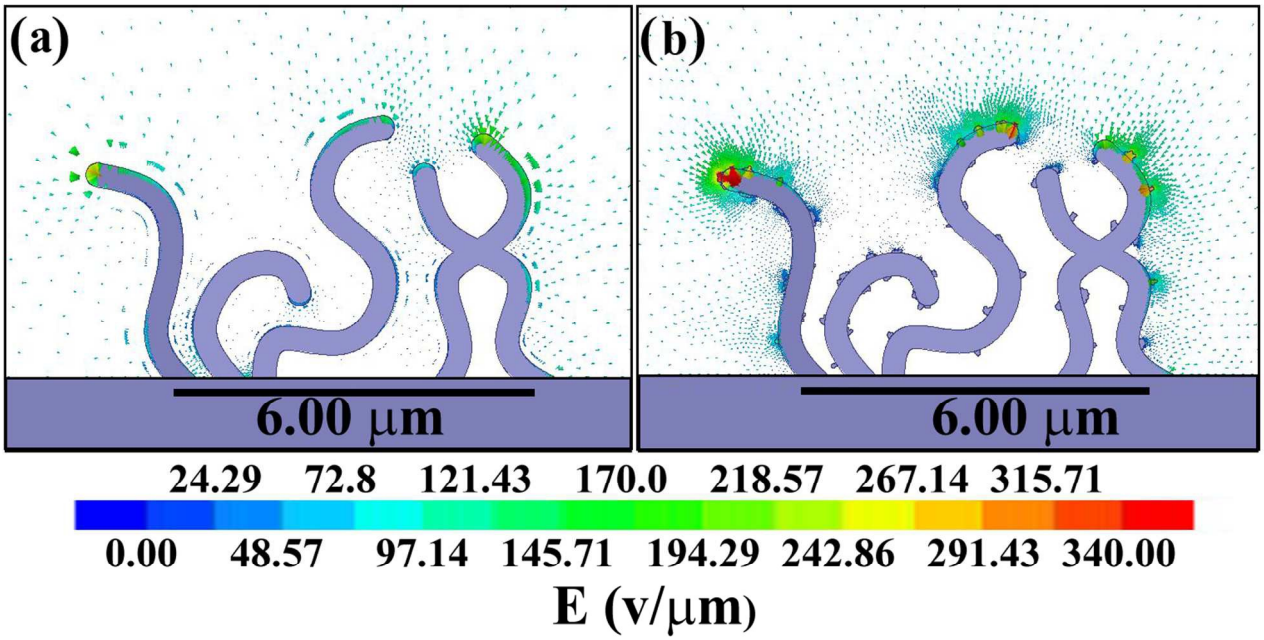

Figure 6. Color vector images of simulated results for (a) bare CNFs and (b) CNF-ZnS hybrid system.

images and hence the five individual CNFs having tortuous morphology were placed side by side. The effective area of our simulated model is very small (~280 nm). For simulation of the CNF-ZnS composite system, small ZnS nanoparticles having diameters around ~10-20 nm were taken and placed in clusters on different portions of the outer surface of CNFs. The base

conducting material was chosen to be conducting carbon tape over which both the CNFs and the composite system lay. For the top electrode, stainless steel was selected. The inter-electrode distance in vacuum space was taken to be ~180 μm matching with our experimental value while equipotential high field was applied in between both the electrodes.

Figure 6a and b display simulated results for bare CNF and CNF-RGO respectively. The CNFs are having tortuous structure and in some cases they are entangled to each-other. It is clear from the figures that both samples exhibit good emission. However field density and emission intensity from CNFs after placement of ZnS nano-clusters, is far better compared to bare CNFs. The large field enhancement after composite formation is depicted nicely in both the simulated vector images. It is also notable from the figures that the main reason behind this improvement for CNF-ZnS system is heavy emission from the secondary emitting sites created by ZnS nanoclusters on CNF surface. As can be seen from figure 6a, the emission for bare CNFs has occurred mainly from the CNF tips having a larger tip diameters thus producing low field density. Whereas, for CNF-ZnS composite system figure 6b clearly depicts that along with CNF tips heavy emission is occurring from the ZnS clusters creating much enhanced field density due to their much smaller curvature diameter. The cumulative dense emission generated from all the secondary emitters produced a much larger field emission for CNF-ZnS composite system compared to bare CNFs.

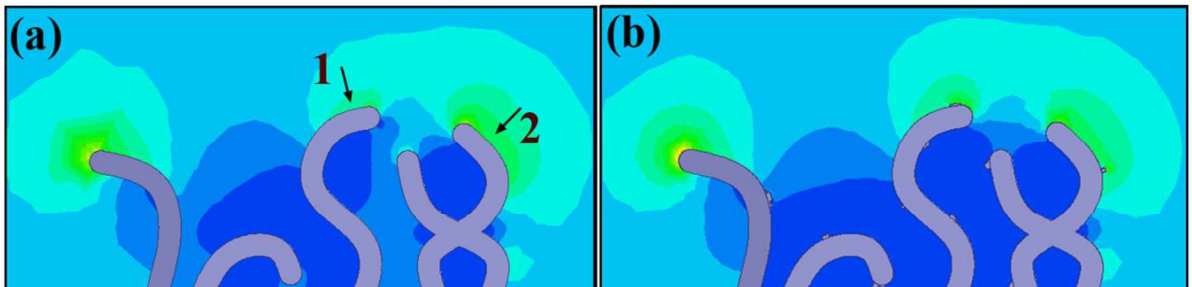

Concentration of ZnS nanoparticles which are attached to the surface of CNFs will definitely affect the field emission property of the nanocomposite. As the ZnS nanoparticles on the surface of the CNF create secondary emission sites, so it is very much evident that the increase of such nanoparticles will in turn generate more emission sites and eventually increase the overall emission of the hybrid system. However, it is difficult to make such kind of gradual increase of the attached- nanoparticles on the outer surface of CNF experimentally. Hence, to find its effect we have carried out some simulation study where the number of ZnS nanoparticles

on the surface of the CNF was changed deliberately and its effect on the electrostatic field distribution was observed carefully. The field distribution is illustrated in figure 7. Weaker field distribution and thereby poor field emission is concluded from pure CNF where no ZnS nanoparticle is attached. However, nanoparticles attached CNFs, exhibited significant increase of emission sites which increase the total emission of the system [figure 7b]. The sites with local field enhancement (emission sites) increases gradually as the numbers of attached ZnS nanoparticles have been deliberately increased and the emission is highest at figure 7d where the number of attachment is highest. Two particular regions in the simulation images are taken and marked [1 and 2 in figure 7a] where the simulated field strengths in each case [m_1 for region 1 and m_2 for region 2] are measured and provided in Table II. As expected, the field strength is the lowest for the configuration shown in figure 7a. As the number of attached nanoparticles is increased in the next configurations, the simulated field strengths have also gradually increased. These results support our previous explanation.

Conclusion:

A CNF-ZnS hybrid composite powder was developed following a simple chemical mixing procedure. The composite material showed excellent luminescence characteristics during PL and CL studies. The CL intensity of the composite was found to be much higher compared to pure ZnS due to incorporation of CNFs and made it a perfect phosphor material for FED application. Again the attachment of ZnS nanoparticles highly improved the field emission characteristics of the composite material and made it an ideal cathode element too for FEDs. For pure CNF the turn-on was found to be 2.1 V/μm whereas for CNF-ZnS composite it reduced to a value of 1.72

V/μm. Altogether, the composite material emerges to be a perfect element to serve dual purpose as both anode and cathode material for FED application.

Acknowledgement:

One of the authors (SK) wants to thank Department of Science and Technology (DST), Govt. of India, for providing him financial support during the execution of the work. We also acknowledge the financial support from the University Grants Commission (UGC), the Govt. of India, also University with potential for excellence (UPEII) scheme.

Sample	Turn on (V/μm)	Maximum Current Density (μA/cm^2)	Field Enhancement factor (β)	
			β_L	β_H
Pure CNF	2.10	9570.4	10047	3184
CNF-ZnS	1.72	16713.4	15427	12324

Table I: Comparison of field emission characteristics between Pure CNF and CNF-ZnS nano-composite.

Table II: Gradual increase of field strength with no. of attached ZnS nanoparticles.

No. of ZnS nanoparticles on CNFs	Amount of field (x 10^8 V/m)	
	m_1	m_2
Nil	1.050	1.271
With 3	1.171	1.300
With 5	1.216	1.368
With all	1.288	1.412

Notes and References:

1. Y. Abdi, S. Mohajerzadeh, H. Hoseinzadegan and J. Koohsorkhi, Carbon nanostructures on silicon substrates suitable for nanolithography, *Appl. Phys. Lett.* 2006, **88**, 053124-3.
2. W. B. Choi, E. Bae, D. Kang, S. Chae, B. Cheong, J. Ko, E. Lee and W. Park, Aligned carbon nanotubes for nanoelectronics, *Nanotechnology*, 2004, **15**, S512–S516.
3. L. Zhang, S. Zaric, X. Tu, X. Wang, W. Zhao and Hongjie Dai, Assessment of Chemically Separated Carbon Nanotubes for Nanoelectronics, *J. Am. Chem. Soc.9*, 2008, **130**, 2686-2691.
4. B. Pradhan, S. K. Batabyal. and A. J. Pal, Functionalized carbon nanotubes in donor/acceptor-type photovoltaic devices, *Appl. Phys. Lett.*, 2006, **88**, 093106.
5. D. D. Nguyen, N. H. Tai, S. Y. Chen and Y. L. Chueh, Controlled growth of carbon nanotube–graphene hybrid materials for flexible and transparent conductors and electron field emitters, *Nanoscale,* 2012, **4**, 632-638.
6. S. Fan, M. G. Chapline, N. R. Franklin, T. W. Tombler, A. M. Cassell and H. Dai, Self-Oriented Regular Arrays of Carbon Nanotubes and Their Field Emission Properties, *Science*, 1999, **283**, 512-514.
7. A. Jha, U. K. Ghorai, D. Banerjee, S. Mukherjee and K. K. Chattopadhyay, Surface modification of amorphous carbon nanotubes with copper phthalocyanine leading to enhanced field emission, *RSC Adv.*, 2013, **3**, 1227-1234.
8. V. Georgakilas, K. Kordatos, M. Prato, D. M. Guldi, M. Holzinger and A. Hirsch, Organic Functionalization of Carbon Nanotubes, *J. Am. Chem. Soc.*, 2002, **124**, 760-761.
9. R. B. Rakhi, A. L. M. Reddy, M. M. Shaijumon, K. Sethupathi and S. Ramaprabhu, Electron field emitters based on multiwalled carbon nanotubes decorated with nanoscale metal clusters, *J Nanopart. Res.*, 2008, **10**, 179-189.

10. D. Tuncel, Non-covalent interactions between carbon nanotubes and conjugated polymers, *Nanoscale*, 2011, **3**, 3545-3554.
11. Y. C. Zhu, Y. Bando, D. F. Xue, Spontaneous growth and luminescence of zinc sulfide nanobelts, *Appl. Phys. Lett.*, 2003, **82**, 1769-1771.
12. R. Vacassy, S. M. Scholz, J. Dutta, H. Hofmann, C. J. G. Plummer, G. Carrot, J. Hilborn and M. Akinc, Nanostructured zinc sulphide phosphors, *MRS Proceedings*, 1997, **501**, 369.
13. T. Igarashia, T. Kusunokia, K. Ohnoa, T. Isobeb, M. Sennab, Degradation proof modification of ZnS-based phosphors with ZnO nanoparticles, *Materials Research Bulletin*, 2001, **36**, 1317–1324.
14. S. W. Kang, B. S. Jeon, J. S. Yoo and J. D. Lee, Optical characteristics of the phosphor screen in field-emission environments, *J. Vac. Sci. Technol. B*, 1997, **15**, 520-523.
15. C. Liu, K. S. Kim, J. Baek, Y. Cho, S. Han, S. W. Kim, N. K. Min, Y. Choi, J. U. Kim and C. J. Lee, Improved field emission properties of double-walled carbon nanotubes decorated with Ru nanoparticles, *Carbon*, 2009, **47**, 1158–1164.
16. S. Shrestha, W. C. Choi, W. Song, Y. T. Kwon, S. P. Shrestha and C. Y. Park, Preparation and field emission properties of Er-decorated multiwalled carbon nanotubes. *Carbon*, 2010 **48**, 54–59.
17. T. Connolly, R. C. Smith, Y. Hernandez, Y. Gun'ko, J. N. Coleman and J. D. Carey, Carbon-Nanotube-Polymer Nanocomposites for Field-Emission Cathodes, *Small*, 2009, **5**, 826–831.
18. R. S. Jayashree, P. V. Kamath, Nickel hydroxide electrodeposition from nickel nitrate solutions: mechanistic studies, *J. Power Sources*, 2001, **93**, 273-278.

19. X. Qi, W. Zhong, Y. Deng, C. Au and Y. Du, Characterization and Magnetic Properties of Helical Carbon Nanotubes and Carbon Nanobelts Synthesized in Acetylene Decomposition over Fe–Cu Nanoparticles at 450 °C*, J. Phys. Chem. C*, 2009, **113**, 15934-15940.

20. ZCPDS card no. 772100.

21. N. K. Abbas, K. T. Al- Rasoul and Z. J. Shanan, New Method of Preparation ZnS Nano size at low pH, *Int. J. Electrochem. Sci.*, 2013, **8**, 3049 – 3056.

22. S. Martínez, I. Gómez, M. Hinojosa, O. V. Kharissova and T. Hernández, Highly Luminescent ZnS Nanoparticles Obtained by Microwave Heating. *Synthesis and Reactivity in Inorganic, Metal-Organic, and Nano-Metal Chemistry*, 2010, **40**, 455–464.

23. R. H. Fowler, L. Nordheim, Electron emission in intense electric fields, *Proc. Roy .Soc. Lond A*, 1928, **119**, 173-181.

24. N. S. Ramgir, D. J. Late, A. B. Bhise, I. S. Mulla, M. A. More, D. S. Joag and V. K. Pillai, Field emission studies of novel ZnO nanostructures in high and low field regions, *Nanotechnology*, 2006, **17**, 2730–2735.

25. N. S. Ramgir, D. J. Late, A. B. Bhise, M. A. More, I. S. Mulla, D. S. Joag and K. Vijayamohanan, ZnO Multipods, Submicron Wires, and Spherical Structures and Their Unique Field Emission Behavior. *J. Phys. Chem. B*, 2006, **110**, 18236-18242.

26. C. J. Edgcombe, U. Valdre, Microscopy and computational modelling to elucidate the enhancement factor for field electron emitters, *Journal of Microscopy*, 2001, **203**, 188-194.

27. J. W. G. Wilder, L. C. Venema, A. G. Rinzler, R. E. Smalley, and C. Dekker, Electronic structure of atomically resolved carbon nanotubes, *Nature (London)*, 1998, **391**,59-62.

28. K. Yu, Y. S. Zhang, F. Xu, Q. Li, Z. Q. Zhu and Q. Wan, Significant improvement of field emission by depositing zinc oxide nanostructures on screen-printed carbon nanotube films, *Appl. Phys. Lett.*, 2006, **88**, 153123-3.

29. Y. Yang, S. Xue, S. Liu, J. Huang and J. Shen, Fabrication and characteristics of ZnS nanocrystals/polymer composite doped with tetraphenylbenzidine single layer structure lightemitting diode, *Appl. Phys. Lett.*, 1996, **69** (3), 377-379.

30. W. Yi, T. Jeong, S. G. Yu, J. Heo, C. Lee, W. Kim, J. B. Yoo and J. Kim, Field-Emission Characteristics from Wide-Bandgap Material-Coated Carbon Nanotubes, Adv. Mater., 2002, **14,** 1464-1468.

31. Y. M. Ho, W. T. Zheng, Y. A. Li, J. W. Liu and J. L. Qi, Field Emission Properties of Hybrid Carbon Nanotube-ZnO Nanoparticles, *J. Phys. Chem. C*, 2008, **112**, 17702-17708.

32. T. Yokogawa, T. Ishikawa and J. L. Merz, Spectroscopic characterization of band discontinuity in free-standing CdZnS/ZnS strained layer superlattices, *J. Appl. Phys.*, 1994, **75(4)**, 2189-2193.

33. N. T. Gurin, A. M. Afanas'ev, O. Yu. Sabitov and D. V. Ryabov, Tunneling and Impact Ionization in Thin-Film ZnS:Mn-Based Electroluminescent Structures, *Semiconductors*, 2006, **40** (8), 920-933.